NJC

ROYAL SOCIETY OF CHEMISTRY

PAPER

View Article Online
View Journal | View Issue

Cite this: *New J. Chem.*, 2025, **49**, 5352

Regulation of color tunability of Dy^{3+}/Eu^{3+}-based double molybdate phosphors with high thermal stability

Mingjie Dan,†[ab] Chonghui Niu,†[ab] Yi Yu,*[ab] Xiurong Zhu,[abc] Wen Zhang,[a] Huan Ye,[a] Zishan Li,[a] Yeqing Wang[d] and Kenneth R. Poeppelmeier*[e]

In this paper, a series of $NaLu(MoO_4)_2$:Dy^{3+} green phosphors and $NaLu(MoO_4)_2$:Dy^{3+},Eu^{3+} multi-color tunable phosphors were prepared by an EDTA–2Na assisted hydrothermal method. The emission of Dy^{3+} ions at two characteristic peaks at 469 nm and 573 nm was observed for the $NaLu(MoO_4)_2$:xDy^{3+} phosphor excited at 355 nm. Through calculation and data fitting, the concentration quenching of Dy^{3+} ions in the $NaLu(MoO_4)_2$ lattice is dominant due to the dipole–dipole interaction. The variable temperature emission spectra show that the luminescence intensity of the $NaLu(MoO_4)_2$:$0.01Dy^{3+}$ phosphor at 423 K decreases to 59% of that at 298 K, while the $NaLu(MoO_4)_2$:$0.01Dy^{3+}$,$0.07Eu^{3+}$ phosphor at 423 K remains at 97% compared to that at room temperature, indicating that the thermal stability of the phosphor is greatly improved by the introduction of Eu^{3+} ions. In addition, by adjusting the ratio of Dy^{3+} to Eu^{3+} ions in the host, the luminescence color gradually changes from green to yellow and finally to orange-red, providing insights into color tuning in the visible range toward various applications. In summary, the Dy^{3+} and Eu^{3+} co-doped $NaLu(MoO_4)_2$ phosphor is a phosphor with good optical properties and excellent thermal stability, which can achieve color tunability and has potential application prospects in the fields of color display and lighting.

Received 4th January 2025,
Accepted 26th February 2025

DOI: 10.1039/d5nj00044k

rsc.li/njc

1. Introduction

Rare earth luminescent materials have great application value in optoelectronic devices, white light diodes (W-LED), solar cells, optical temperature sensors, biomedicine and other fields due to their advantages of high conversion efficiency, narrow-band emission, long lifetime, and good optical stability. They therefore have sparked intensive interest in the development of luminescent materials with excellent luminous properties and stable physical and chemical properties in recent years.[1–4] It is well known that the luminescent properties of rare earth phosphors are closely related to the crystal field environment in the main crystal lattice, which makes it extremely important to explore novel matrixes with stable structures, excellent properties and effective excitation by doping ions. With excellent luminescence performance and stable physical and chemical properties, molybdate has a wide range of application prospects in photocatalysts, phosphors, lasers, *etc.*, attracting great interest and wide attention from researchers.[5–7] Dy^{3+} ions usually have two distinct characteristic emission peaks in the blue (470–500 nm) and yellow (560–600 nm) regions, which correspond to the $^4F_{9/2} \rightarrow {}^6H_{15/2}$ and $^4F_{9/2} \rightarrow {}^6H_{13/2}$ transitions, respectively.[8,9] Monika *et al.* reported that strong emission was observed for the Dy^{3+} doped Sr_2CeO_4 nanophosphor, and the emission intensity of the phosphor was enhanced by co-doping Li^+ ions.[10] Unfortunately, since Dy^{3+} ions lack the characteristic emission in the red region in addition to the blue and yellow components, the color rendering index (CRI) for the Dy^{3+}-based phosphors is very low, far from that demanded for practical luminescent materials.[11,12] To address this problem, another active center with red luminescence is often introduced into the Dy^{3+}-based luminescent materials to compensate for the red composition. In this regard, the Eu^{3+} ion is an ideal option because of its orange and red emission originating from $^5D_0 \rightarrow {}^7F_J$ (J = 1, 2, 3, 4) transitions.[13] Many successes have been achieved by adopting this strategy recently. Liu *et al.*, for instance, synthesized a series of Dy^{3+}/Eu^{3+} co-doped $KLa(MoO_4)_2$ phosphors by a hydrothermal

[a] *School of Physics and Electronic Information, Gannan Normal University, Ganzhou, 341000, Jiangxi, China. E-mail: yuyignnu@163.com*
[b] *Advanced Energy Storage & Photoelectric Materials Research Center, Gannan Normal University, Ganzhou, 341000, Jiangxi, China*
[c] *Shanghai Key Laboratory of Special Artifcial Microstructure Materials & Technology, Department of Physics, Tongji University, Shanghai, 200092, China*
[d] *Department of Applied Physics, East China Jiaotong University, Nanchang, 330013, Jiangxi, China*
[e] *Department of Chemistry, Northwestern University, Evanston, Illinois, 60208, USA. E-mail: krp@northwestern.edu*
† These authors contributed equally to this work.

method[14] and they exhibited high multi-color tunable ability from the yellow to red region, crossing the white light area, indicating that this sort of phosphor has broad application prospects in white diodes, full-color displays, photoelectric devices and other fields. Devakumar *et al.* prepared a series of color-tunable Dy^{3+}/Eu^{3+} co-doped $CsGd(MoO_4)_2$ (CGM) phosphors *via* a high temperature solid phase reaction.[15] The combination of the comprehensive analysis of the crystal structure, morphology, vibration mode, luminescence characteristics and energy transfer mechanism manifests the fact that the emission color of the phosphor can be easily tuned by altering the content ratio of Dy^{3+} to Eu^{3+}. Zhang *et al.* prepared the Gd-MOF:Eu^{3+},Dy^{3+} phosphors and investigated the temperature sensing properties in the temperature range of 213–453 K. The luminescence color of this phosphor varied from yellow to red as the temperature increased.[16] Wan *et al.* prepared Dy^{3+}/Eu^{3+} co-doped $Sr_2Ga_2GeO_7$ (SGGO) phosphors with different concentrations of Eu^{3+} by a high temperature solid phase method.[17] Under 344 nm excitation, the emission intensity of Dy^{3+} was attenuated and the emission lifetime was shortened. In contrast, the lifetime of Eu^{3+} was increased. Such a confirmation of energy transfer from Dy^{3+} to Eu^{3+} in the Dy^{3+}/Eu^{3+}:SGGO phosphors endows them with huge potential application in plant growth as tunable orange radiation resources. Inspired by these studies, a series of Dy^{3+} single-doped and Dy^{3+}/Eu^{3+} co-doped $NaLu(MoO_4)_2$ (NLMO) phosphors were prepared by an EDTA–2Na-assisted hydrothermal method in this paper. The phase purity, morphology, luminescence and thermal stability of the as-synthesized phosphors were studied in detail. The color purity and correlated color temperature (CCT) of the phosphor were calculated and plotted in the Commission Internationale de L'Eclairage (CIE) coordinate diagram, indicating good color characteristics in this studied system. The energy transfer processes between Dy^{3+} and Eu^{3+} ion luminescence centers were explored, too. All the results demonstrated that high efficiency multi-color tunable emission, starting from green to orange and then to red could be easily realized *via* varying the concentration of Eu^{3+} in the NLMO:Dy^{3+}/Eu^{3+} phosphors, indicating their prominent potential applications in the fields of color display and lighting.

2. Experiment

2.1. Synthesis

A series of NLMO:$x$$Dy^{3+}$ (x = 0, 0.01, 0.03, 0.06, 0.09, 0.15, and 0.20) and NLMO:0.1Dy^{3+},$y$$Eu^{3+}$ (y = 0.005, 0.01, 0.07, 0.13, and 0.19) phosphors were prepared by an EDTA–2Na assisted hydrothermal method. $Na_2MoO_4{\cdot}2H_2O$ with A.R. grade and $Lu(NO_3)_3{\cdot}6H_2O$, $Dy(NO_3)_3{\cdot}6H_2O$, as well as $Eu(NO_3)_3{\cdot}6H_2O$ with the purity of 99.99% were employed as raw materials. $C_{10}H_{14}N_2O_8Na_2{\cdot}2H_2O$(A.R.) was adopted as an active agent to better control the morphology of the sample and improve the luminescence performance. For a typical preparation process, a stoichiometric amount of $Na_2MoO_4{\cdot}2H_2O$ (0.006 mol) was dissolved in 10 ml of deionized water and stirred for 20–30 minutes to form solution A. An overall amount of 0.003 mol of $Ln(NO_3)_3{\cdot}6H_2O$ (Ln = Lu, Dy, and Eu) was weighed and dissolved in 10 ml of deionized water while stirring for 15–30 minutes to form solution B. Subsequently, 0.003 mol EDTA–2Na was dissolved in 10 ml of deionized water to form a solution at lower temperature (60–80 °C) for about 60 minutes to ensure the homogeneity of the solution. Then, solution C was added to solution B, resulting in the immediate appearance of white precipitates. The mixed solution was stirred for about 20 minutes. Sequentially, the precipitate was poured to solution A to form a suspension and stirred for another 20 minutes. Next, the mixture was transferred to a Teflon-lined autoclave with a capacity of 50 mL and the temperature was kept at 180 °C for 12 hours. After naturally cooling to room temperature, the product was centrifuged and washed with deionized water several times. Finally, the white sediment was dried at 80 °C for 5 hours and then calcined at 800 °C for 2 hours in a muffle furnace.

2.2. Measurements and characterization

A high-resolution X-ray powder diffractometer (Bruker D8 Advance) with monochromatic Cu Kα radiation (λ = 0.15406 nm) was used for the PXRD measurement with the 2θ over the range of 15–65° with the step of 0.01°. The morphology of the samples was characterized using an FEI Quanta 400 thermal field emission scanning electron microscope (SEM). The photoluminescence (PL) and photoluminescence excitation (PLE) spectra were analyzed using a Hitachi 2500 fluorescence spectrometer equipped with a 150 W xenon lamp as a light source. The temperature-dependent emission spectrum (T = 298–473 K) and decay lifetimes of the samples were measured with an Edinburgh FLS980 spectrometer under an alternating light source of 150 W xenon and pulsed xenon lamps.

3. Results and discussion

3.1. Crystal structure, phase and morphology analysis

Fig. 1(a) and (b) show the XRD patterns for the NLMO:$x$$Dy^{3+}$ (x = 0, 0.01, 0.03, 0.06, 0.09, 0.15, and 0.20) and NLMO:0.01-Dy^{3+},$y$$Eu^{3+}$ (y = 0.005, 0.01, 0.07, and 0.13, 0.19) phosphors, respectively. All the patterns are consistent with that for the standard (PDF#23-1192), with no existence of heterophase, demonstrating not only the effectivity of the preparation method adopted in this study but also the high structural tolerance of the host matrix toward rare-earth ion substitution. According to the theory of defect chemistry, the position occupied by the doping elements in the host lattice can be estimated by the percentage difference (D_r) of the ionic radii, which can be expressed as follows:[18]

$$D_r \approx \left[\frac{R_m(CN) - R_d(CN)}{R_m(CN)}\right] \times 100\% \quad (1)$$

where R_m and R_d are the radii of the host ion and doping ion, respectively, CN is the coordination number which is 8 for the concerned site according to the structure information of the NLMO matrix. Generally, the probability of the doping ion to replace the host ion is inversely proportional to the value of D_r, and therefore, a smaller value of D_r means an easier occurrence of replacement. Based on formula (1), the D_r values for the case

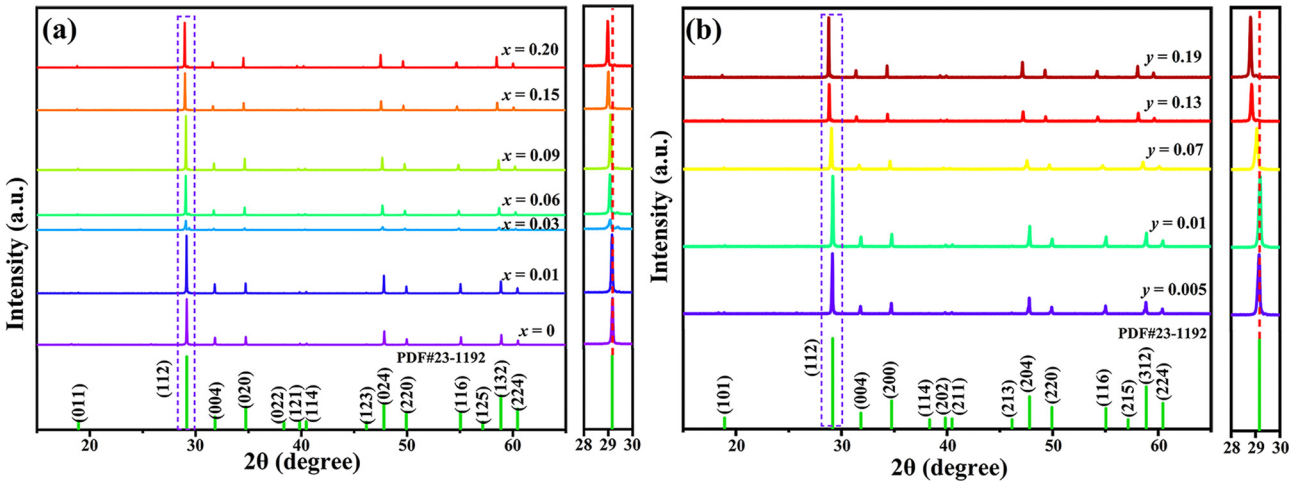

Fig. 1 PXRD patterns for (a) NLMO:xDy^{3+} (x = 0, 0.01, 0.03, 0.06, 0.09, 0.15, and 0.20) and (b) NLMO:0.01Dy^{3+},yEu^{3+} (y = 0.005, 0.01, 0.07, 0.13, and 0.19) phosphors.

of Dy^{3+} replacing Lu^{3+} and Na^{+} are 10.3% and 12.7%, respectively. Therefore, it is rational to assume that the Dy^{3+} ions will substitute Lu^{3+} other than Na^{+} while maintaining the host structure even with a relatively high doping concentration. It is notable that the introduction of Dy^{3+} has resulted in a certain degree of unit cell expansion and reduction of the distance between two randomly adjacent Miller faces of the main lattice without damaging the structure. As the concentration of Dy^{3+} increases, the XRD diffraction peaks shift to the lower angle side compared with the standard pattern, which is illustrated in the inset along with Fig. 1(a). The shift of the diffraction peaks for the Dy^{3+}/Eu^{3+} co-doped samples were larger compared to those for the Dy^{3+} single doped ones (Fig. 1(b)). This is mainly ascribed to the larger radius of Eu^{3+} ions (1.07 Å) than that of Dy^{3+} ions (1.03 Å) and both of which are larger than that of Lu^{3+} ions (0.97 Å). When Dy^{3+} or Eu^{3+} ions enter the host lattice, their larger radius will inevitably cause the expansion of the unit cell. This is well in line with the Bragg diffraction equation known as $2d \sin\theta = n\lambda$. The expansion leads to the increase of distance between two adjacent Miller faces, and in the meantime, the diffraction peaks would shift to the lower angle side. Such good agreement between experimental results and theoretical expectation further confirms easy-doping of Dy^{3+} and Eu^{3+} ions in the NLMO lattice,[19] providing an opportunity of regulating the luminescence color of the phosphors in a vast range and easy way.

Fig. 2(a) and (b) show the SEM images of NLMO:0.01Dy^{3+} phosphors at different magnification rates. It can be observed from the images that the particles show good morphology with regular pie-like shape and good uniformity. A large proportion of the particles have very similar diameters which are estimated to be 3–4 μm, further indicating the effectiveness of the synthesis method and the specific parameters adopted for sample preparation. For phosphors that are focused on their optical performances, the morphology is one of the important factors. Therefore, the good morphology of the studied sample boosts its attractive optical properties.

3.2. Photoluminescence properties

Fig. 3(a) shows the emission spectra of NLMO:xDy^{3+} (x = 0, 0.01, 0.03, 0.06, 0.09, 0.15, 0.20) phosphors over the range of 445–630 nm excited at 390 nm. Due to the $^{4}F_{9/2} \rightarrow {}^{6}H_{13/2}$ transition of Dy^{3+}, the spectra exhibit a strong yellow emission around 575 nm. Other two additional weak emission bands located at

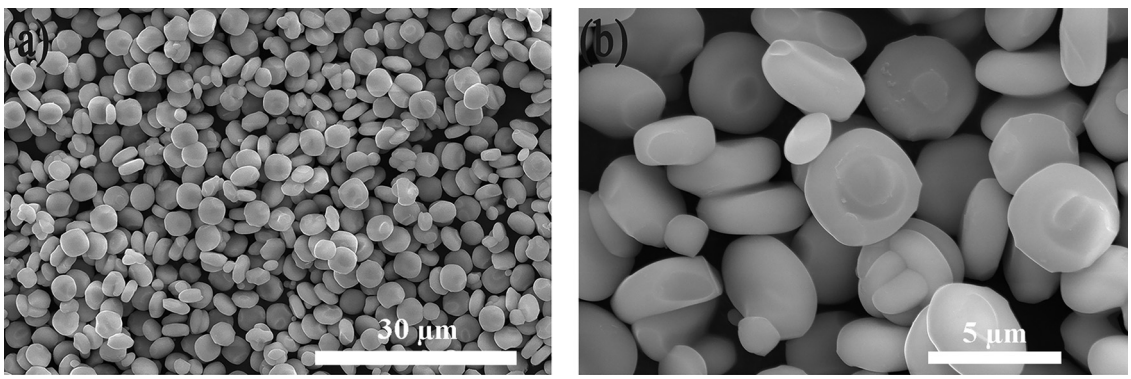

Fig. 2 SEM images of NLMO:0.01Dy^{3+} phosphors with (a) low-magnification and (b) high-magnification, respectively.

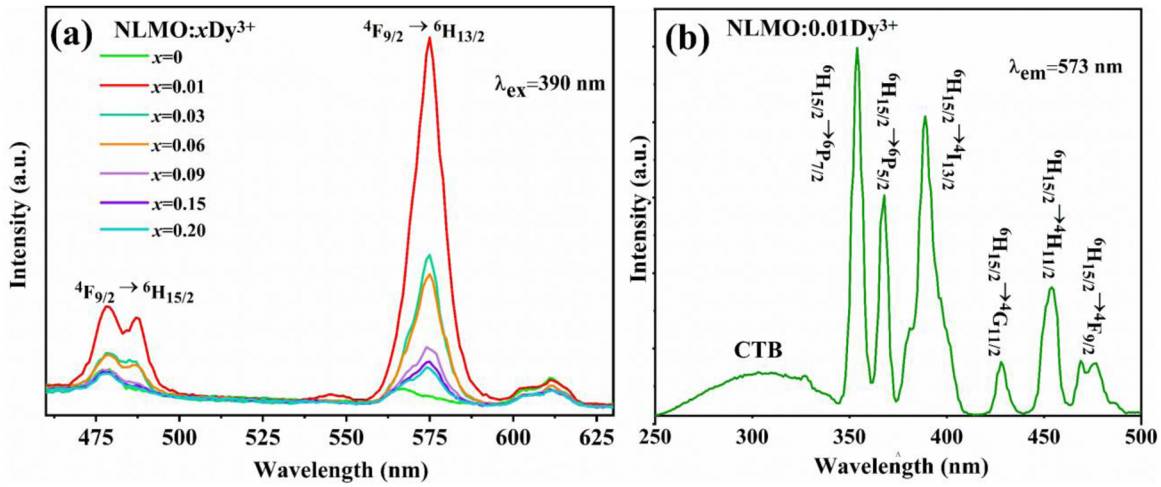

Fig. 3 (a) PL spectra of NLMO:xDy^{3+} (x = 0, 0.01, 0.03, 0.06, 0.09, 0.15, and 0.20) phosphors and (b) PLE spectrum of the NLMO:0.01Dy^{3+} phosphor.

490 nm and 611 nm which correspond to $^4F_{9/2} \rightarrow {}^6H_{15/2}$ and $^4F_{9/2} \rightarrow {}^6H_{11/2}$ are observed.[20] The blue emission belongs to the magnetic dipole transition which is insensitive to the local environment, while the yellow emission is a super-sensitive electric dipole transition, whose intensity is significantly affected by the crystal field around Dy^{3+} ions.[21] This characteristic implies that it is highly possible to achieve color-tunable light in this monotype phosphor by varying the concentration of the dopant. In general, the yellow emission predominates when Dy^{3+} occupies at a non-inverted center. In contrast, the blue emission will be stronger when Dy^{3+} is located at a highly symmetric position. Hence, the strong yellow emission at 573 nm for the NLMO:xDy^{3+} series indicates that Dy^{3+} ions occupy a low symmetric site in the NLMO main lattice with no inversion center. In addition, with the increase of Dy^{3+} concentration, the yellow emission intensity gradually increases and it reaches the summit at x = 0.01. Then it began to significantly decline due to the concentration quenching effect with the further increase of Dy^{3+} concentration. The cross relaxation (CR) mechanism originating from the resonance energy transfer (ET) between adjacent Dy^{3+} ions is likely responsible for this effect.[22] The PLE spectra of NLMO:0.01Dy^{3+} phosphors monitored at 573 nm are shown in Fig. 3(b). The PLE spectrum consists of a weak wide $O^{2-} \rightarrow Mo^{6+}$ charge transfer (CT) band in the region of 200–350 nm and other 6 sharp peaks located at 351, 366, 390, 426, 453, and 472 nm corresponding to $^6H_{15/2} \rightarrow {}^6P_{3/2}$, $^6H_{15/2} \rightarrow {}^6P_{7/2}$, $^6H_{15/2} \rightarrow {}^6P_{5/2}$, $^6H_{15/2} \rightarrow {}^4I_{13/2}$, $^6H_{15/2} \rightarrow {}^4G_{11/2}$, $^6H_{15/2} \rightarrow {}^4H_{11/2}$ and $^6H_{15/2} \rightarrow {}^4F_{9/2}$ transitions, respectively.[23] There is a weak excitation peak at about 328 nm ascribed to the $^6H_{15/2} \rightarrow {}^4G_{9/2}$ transition combined with the CT band. Obviously, the excitation intensities at 351 nm and 390 nm are stronger than those of the other peaks, indicating that the samples are the most suitable to be excited at these wavelengths. Considering that light at 390 nm is more commercially available than the light at 351 nm, we used 390 nm to excite a single-doped sample.

In order to better reveal the concentration quenching mechanism of the NLMO:Dy^{3+} phosphor, the calculation of critical distance (R_c) which is given by the following formula is a common but helpful method:[24,25]

$$R_c \approx 2\left[\frac{3V}{4\pi x_c Z}\right]^{\frac{1}{3}} \quad (2)$$

where V is the volume of a single cell, Z represents the number of replaceable cations in the host matrix in a unit cell, and x_c is the critical concentration of the activator. For the NLMO matrix, V = 299.4 Å^3, x_c = 0.01, and Z = 2. As such, the value of R_c is 19 Å, which is much larger than 5 Å, demonstrating that the concentration quench effect is derived from the multipolar interaction. Furthermore, the exact type of interaction can be determined by using Dexter's theory which is expressed as follows:[26,27]

$$\log\left(\frac{I}{x}\right) = A - \frac{Q}{3}\log(x) \quad (3)$$

where I is the emission intensity, x is the doping concentration, A is a constant, and Q may be 6, 8, and 10 corresponding to dipole–dipole, dipole–quadrupole, and quadrupole–quadrupole interactions, respectively. Based on the emission spectra, $\log(I/x)$ as a function of $\log(x)$ is shown in Fig. 4. After linear fitting, the slope is −1.77 and consequently the calculated Q value is 5.6 which is very close to 6, demonstrating that the Dy^{3+} ion concentration quenching in the NLMO matrix is mainly caused by dipole–dipole interaction.

Since the optical properties of NLMO:0.01Dy^{3+} are not ideal for the color tunable applications, Eu^{3+} is usually co-incorporated with Dy^{3+} to improve the optical performance. In this regard, a series of NLMO:0.01Dy^{3+},yEu^{3+} (y = 0.005, 0.01, 0.07, 0.13, 0.19) phosphors were prepared by the same method mentioned above. Fig. 5 shows the difference between PLE spectra of NLMO:0.01Dy^{3+},yEu^{3+} phosphors monitored at 573 nm and 614 nm, respectively. As depicted in Fig. 5(a), the shapes and locations of the excited bands are similar to those appearing in the PLE spectra of Dy^{3+}-single doped NLMO phosphors. However, the intensities corresponding to the

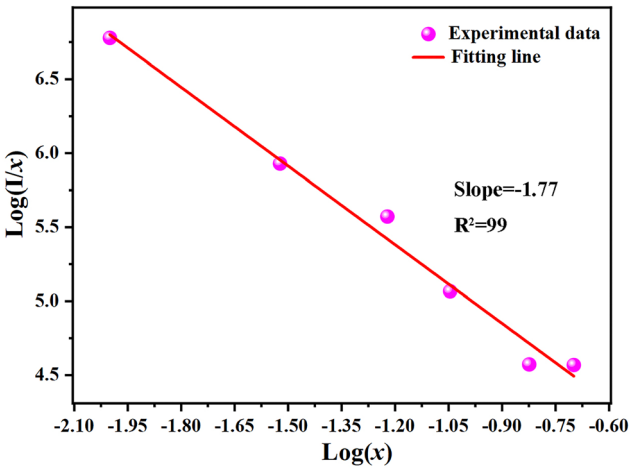

Fig. 4 Dependency of log(*I*/*x*) on log(*x*).

excitation peaks gradually decrease as the concentration of Eu^{3+} rises. This implies that there should exist energy transfer from Dy^{3+} to Eu^{3+} activator. Interestingly, the CT band over 240–340 nm also deteriorates after Eu^{3+} was introduced. This may be because of the increase of Mo–O bond distance caused by unit cell expansion, which makes the charge transition between O^{2-} and Mo^{6+} more difficult than the case without Eu^{3+} doped. In contrast, the PLE spectra monitored at 614 nm, as shown in Fig. 5(b), have strong and broad absorption bands, which is attributed to the overlap between $Mo^{6+} \rightarrow O^{2-}$ and $Eu^{3+} \rightarrow O^{2-}$ charge transfer transitions.[28] Particularly, as the former transition was gradually weakened, the latter transition should dominantly contribute to the band. What's more, because Eu^{3+} has high probability of red light emission at about 614 nm, the absorbed energy can be quickly released in the form of red light, leading to the significant boost of absorption ability of this phosphor within the 240–340 nm range. Other several narrow peaks, centered at 361 ($^7F_0 \rightarrow {}^5D_4$), 375 ($^7F_0 \rightarrow {}^5G_2$), 380 ($^7F_0 \rightarrow {}^5G_3$), 393 ($^7F_0 \rightarrow {}^5L_6$), 415 ($^7F_0 \rightarrow {}^5D_3$) and 464 nm ($^7F_0 \rightarrow {}^5D_2$) were observed. These peaks belong to the characteristic f–f transition of Eu^{3+} ions. In addition, relative weak peaks at 351, 366, 426, and 453 nm, corresponding to $^6H_{15/2} \rightarrow {}^6P_{7/2}$, $^6H_{15/2} \rightarrow {}^6P_{5/2}$, $^6H_{15/2} \rightarrow {}^4G_{11/2}$, and $^6H_{15/2} \rightarrow {}^4H_{11/2}$ transitions of Dy^{3+} are still present in the NLMO:*x*Dy^{3+} phosphors.[23] It is notable that the intensity at 393 nm is comparable to that at 355 nm, implying that the NLMO:0.01Dy^{3+},*y*Eu^{3+} phosphors are appropriate to be excited at both wavelengths. What's more, the excitation intensities present a monotonically increasing trend with the ascent of Eu^{3+} concentration, but the increasing rate becomes significantly slow when the Eu^{3+} concentration exceeds 7 at%, suggesting that the appropriate concentration of Eu^{3+} might be at this doping level.

Fig. 6(a) shows the PL spectra of NLMO:0.01Dy^{3+},*y*Eu^{3+} (*y* = 0.005, 0.01, 0.07, 0.13, and 0.19) phosphors under the excitation at 355 nm. When compared to the Dy^{3+}-single doped NLMO samples, the PL spectra of NLMO:0.01Dy^{3+},*y*Eu^{3+} maintain distinct emission bands at 486 nm and 573 nm, which correspond to the $^4F_{9/2} \rightarrow {}^6H_{15/2}$ and $^4F_{9/2} \rightarrow {}^6H_{13/2}$ transitions of Dy^{3+}. However, their intensities are weakened dramatically. Conversely, the emission intensity at 614 nm experiences a notable enhancement due to the combination of $^5D_0 \rightarrow {}^7F_2$ transition of Eu^{3+} and $^4F_{9/2} \rightarrow {}^6H_{11/2}$ transition of Dy^{3+}. Additionally, two weaker emission peaks at 655 nm and 703 nm are also observed, which can be ascribed to the $^5D_0 \rightarrow {}^7F_3$ and $^5D_0 \rightarrow {}^7F_4$ transitions of Eu^{3+}, respectively. In addition, as the concentration of Eu^{3+} increases, both the emissions at 486 nm and 573 nm monotonously decrease while the emission at 614 nm first increases and then decreases with the highest intensity at *y* = 0.07, as illustrated in Fig. 6(b). Excessive concentration of Eu^{3+} won't continuously boost and will even reduce the red light emission. This is likely due to the shortened distance between two adjacent Eu^{3+} ions when a larger amount of Eu^{3+} ions is incorporated, consequently enhancing the nonradiative relaxation process. Such considerable variations in PL spectral emission intensities of Dy^{3+} and Eu^{3+} in the NLMO:0.01Dy^{3+},*y*Eu^{3+} (*y* = 0.005, 0.01, 0.07, 0.13, and 0.19) phosphors indicate that energy transfer and multicolor tunable emission among blue, yellow and red emissions can be realized by appropriately adjusting the ratio of Dy^{3+} and Eu^{3+} ion concentration.[29]

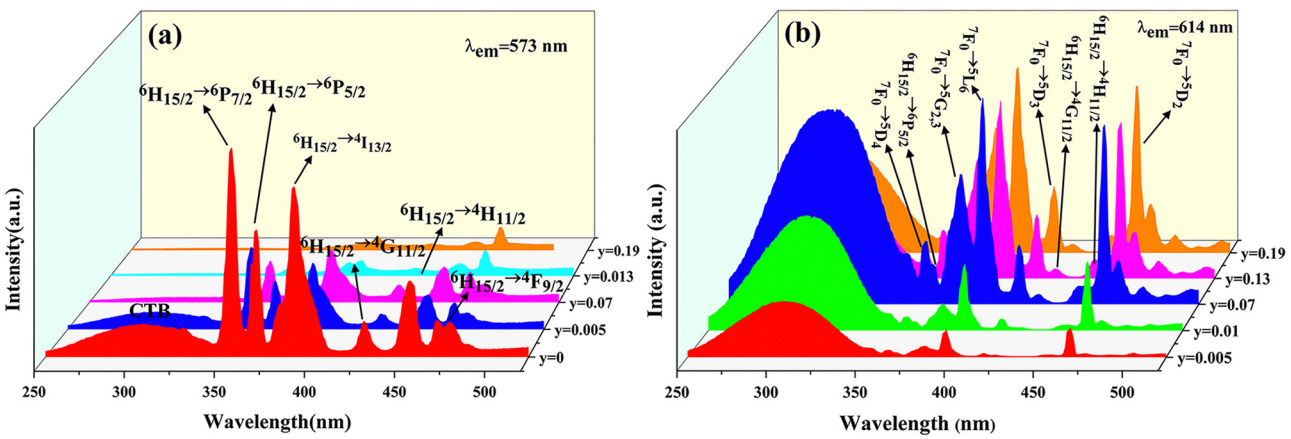

Fig. 5 PLE spectra of NLMO:0.01Dy^{3+},*y*Eu^{3+} (*y* = 0.005, 0.01, 0.07, 0.13, and 0.19) phosphors monitored at 573 and 614 nm, respectively.

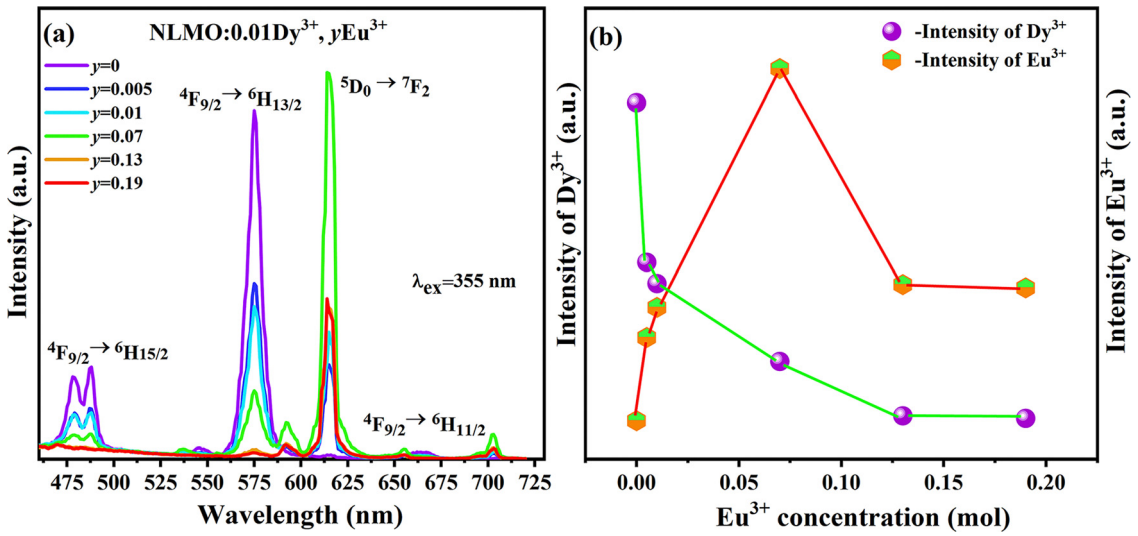

Fig. 6 (a) PL spectra of NLMO:0.01Dy^{3+},yEu^{3+} (y = 0.005, 0.01, 0.07, 0.13, and 0.19) phosphors; (b) line chart of emission intensity changes at 573 nm and 614 nm as the function of Eu^{3+} concentration.

To uncover the energy transfer process between Dy^{3+} ions and Eu^{3+} ions, an in-depth investigation was conducted into the emission lifetimes of NLMO:0.01Dy^{3+},yEu^{3+} (y = 0, 0.005, 0.01, 0.07, 0.13, 0.19) phosphors. Fig. 7 shows the attenuation curves excited at 355 nm and monitored at 573 nm. For fitting calculations, a double exponential formula was utilized, as detailed below:[30]

$$I_t = I_0 + A_1 \exp\left(-\frac{t}{\tau_1}\right) + A_2 \exp\left(-\frac{t}{\tau_2}\right) \quad (4)$$

where I_t is the luminescence intensity varying with time, and A_1 and A_2 are constants. Thus, the average life can be calculated by the following formula:[31,32]

$$\tau_{ave} = \frac{A_1\tau_1^2 + A_2\tau_2^2}{A_1\tau_1 + A_2\tau_2} \quad (5)$$

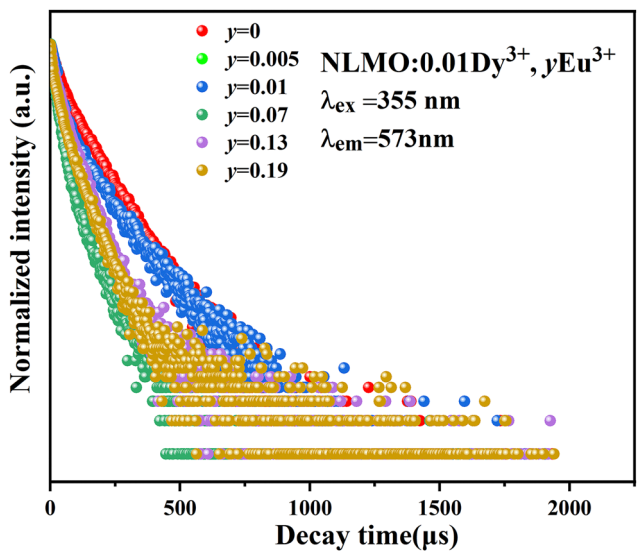

Fig. 7 Decay curves for the NLMO:0.01Dy^{3+},yEu^{3+} (y = 0.005, 0.01, 0.07, 0.13, and 0.19) phosphors.

Then, the lifetimes of the NLMO:0.01Dy^{3+}yEu^{3+} (y = 0, 0.005, 0.01, 0.07, 0.13, and 0.19) phosphors are 94, 79.4, 61.9, 39.7, 10.53 and 9.12 μs, respectively. Obviously, the lifetime of Dy^{3+} decreases in turn with the increase of Eu^{3+} ion concentration, which resulted in a shortened distance between Dy^{3+} and Eu^{3+} ions, which facilitates the Dy^{3+} → Eu^{3+} energy transfer and subsequently reduces the emission lifetime of Dy^{3+} ions. Furthermore, the efficiency of energy transfer η_τ also rises in line with the increase of Eu^{3+} concentration, which can be estimated by employing the following formula:[33]

$$\eta_\tau = 1 - \frac{\tau}{\tau_0} \quad (6)$$

where τ and τ_0 are the emission lifetimes of Dy^{3+} ions when Eu^{3+} is co-doped or not, respectively. Through this equation, the energy transfer efficiencies of NLMO:0.01Dy^{3+} and NLMO:0.01-Dy^{3+},yEu^{3+} phosphors with y varying from 0.005 to 0.19 are 15.64%, 25.5%, 57.79%, 88.82% and 90.32%, respectively.

With the combination of the PL and PLE spectra, as well as the related lifetimes, the mechanism of the energy transfer process in the NLMO:0.01Dy^{3+},yEu^{3+} phosphors was unveiled and is shown in Fig. 8. When excited at 355 nm, electrons of Dy^{3+} at ground state transit to the $^6P_{1/2}$ state. Successively, a proportion of the excited electrons relaxes nonradiatively to the lower $^4F_{9/2}$ state and then transits back to ^6H_J states where J = 15/2, 13/2, and 11/2, accompanied by the light emission at 489, 573, and 678 nm, respectively. Meanwhile, electrons of Eu^{3+} are excited to the $^5D_4$ state and then relax to the $^5D_0$ and $^5D_1$ states, leading to the observation of the characteristic emission of the Eu^{3+} ions corresponding to the $^5D_1$ → $^7F_1$, $^5D_0$ → $^7F_0$, $^5D_0$ → $^7F_1$ and $^5D_0$ → $^7F_2$ transitions. Furthermore, with the help of energy transition from $^4F_{9/2}$ state of Dy^{3+} to $^5D_0$ and $^5D_1$ states of Eu^{3+}, the number of electrons at these two states sharply increases, and as a consequence, the emission of the Eu^{3+} is amplified, especially for the emission at 614 nm.

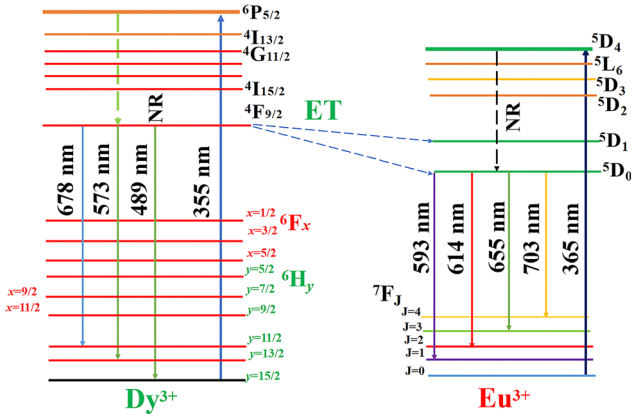

Fig. 8 Schematic diagram of electron transition and energy transfer in the Dy^{3+}/Eu^{3+} co-doped NLMO phosphors.

3.3. Thermal stability

The application of phosphors in W-LED lighting hinges significantly on their thermal stability. The thermal stability of NLMO:0.01Dy^{3+} and NLMO:0.01Dy^{3+},0.07Eu^{3+} phosphors within the temperature range of 298–473 K has been studied. The fluorescence spectra of these two samples, excited at a wavelength of 355 nm, were recorded at various temperatures and are presented in Fig. 9(a) and (b) respectively. As the temperature increased, the luminescence intensity at 573 nm for NLMO:0.01Dy^{3+} and at 614 nm for NLMO:0.01Dy^{3+},0.07Eu^{3+} phosphors decreased. Specifically, Fig. 9(a) reveals that the NLMO:0.01Dy^{3+} phosphor retained 59% of its initial luminous intensity at 298 K when heated to 423 K. In contrast, the NLMO:0.01Dy^{3+},0.07Eu^{3+} phosphor maintained an impressive 97% of its room temperature luminous intensity at 423 K. Such a remarkable improvement in thermal stability is mainly due to the enhanced structural stability of the matrix caused by the larger radius of Eu^{3+} in comparison to that of Lu^{3+}, and successively, the rigidity of the Lu(Dy/Eu)O_8 polyhedron in the lattice is improved. As we know, higher rigidity generally signifies lower phonon energy and thereby the phonon-assisted nonradiative transition process will be weakened. As a result, the thermal stability is improved. Another factor, cross relaxation is also believed to have influence on the thermal stability issue. As the unit cell expands due to the entrance of Eu^{3+} in the lattice, the occurrence of the cross relaxation process seems to be much more difficult and consequently improves the thermal stability. In addition, the

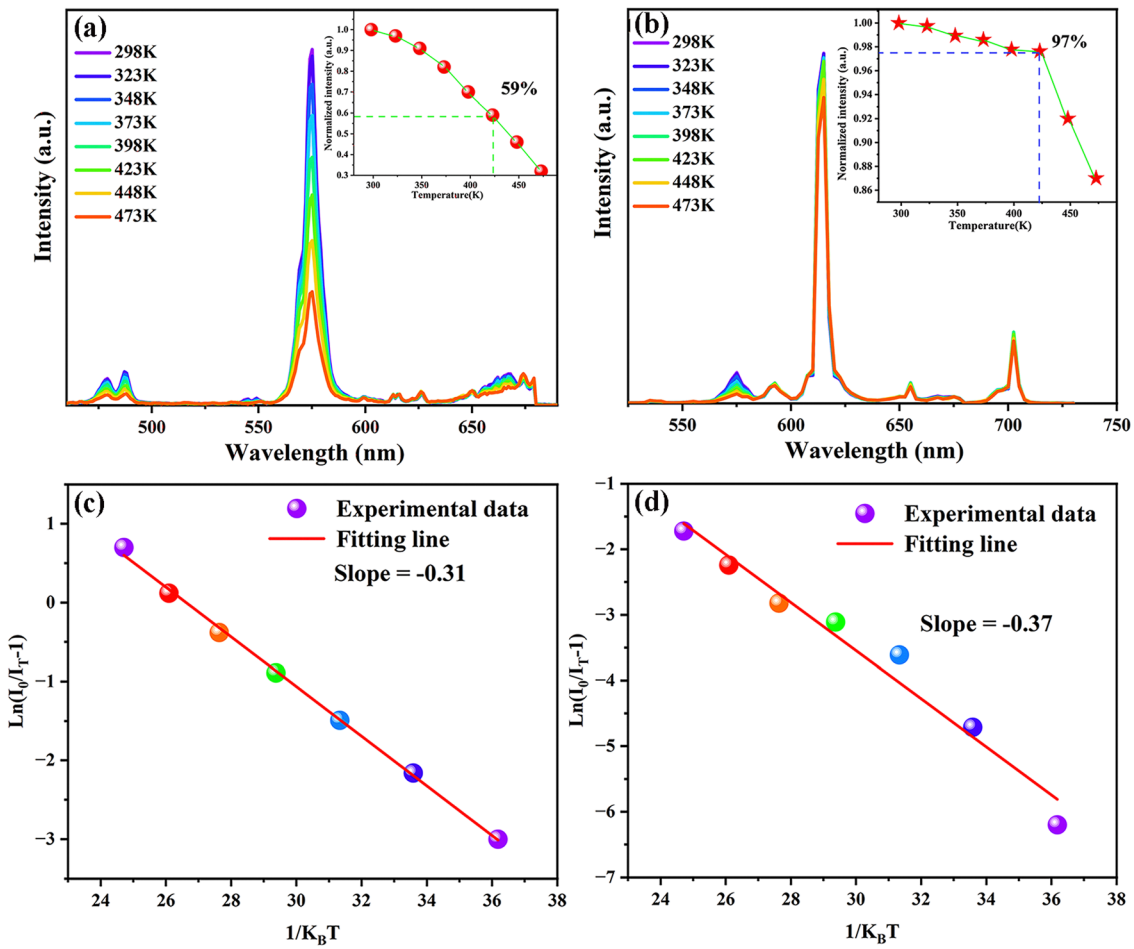

Fig. 9 Temperature-dependent fluorescence spectra for (a) NLMO:0.01Dy^{3+} and (b) NLMO:0.01Dy^{3+},0.07Eu^{3+} phosphors within the temperature range of 298–473 K. The relationship between $\ln(I_0/I_T - 1)$ and $1/K_BT$ for (c) NLMO:0.01Dy^{3+} and (d) NLMO:0.01Dy^{3+},0.07Eu^{3+}.

increased bonding energy is believed to be an important reason for thermal stability development, too. The bonding energy for the NLMO:0.01Dy^{3+} and NLMO:0.01Dy^{3+},0.07Eu^{3+} phosphors can be calculated by the following formula:[34]

$$\ln\left(\frac{I_0}{I_T}-1\right)=\ln A-\frac{\Delta E}{K_B T} \quad (7)$$

where I_0 is the PL intensity at 298 K, I_T is the PL intensity at different temperatures, A is the constant, K_B is the Boltzmann constant, T is the temperature, and ΔE is the activation energy. Thus, as shown in Fig. 9(c) and (d), the $\ln(I_0/I_T-1)$ and $1/K_BT$ for the NLMO:0.01Dy^{3+} and NLMO:0.01Dy^{3+},0.07Eu^{3+} phosphors were linearly fitted, and the slopes for them are −0.31 and −0.37, respectively. This indicates that the substitution of Lu^{3+} by Eu^{3+} promotes the bonding energy from 0.31 eV in NLMO:0.01Dy^{3+} to 0.37 eV in NLMO:0.01Dy^{3+},0.07Eu^{3+} phosphors, and consequently, results in the improvement of the thermal stability of the phosphor.[35] Under the synergistic effect of the factors discussed above, the incorporation of Eu^{3+} ions has markedly enhanced the thermal stability of the phosphor, implying its promising potential for use in white light illumination and color display applications.

3.4. CIE associated color temperature (CCT)

Based on the PL spectra of NLMO:0.01Dy^{3+},yEu^{3+} (y = 0, 0.005, 0.01, 0.07, 0.13, 0.19) phosphors, the CIE chromaticity coordinates for them were calculated and are illustrated in Fig. 10(a), followed by the calculation of color purity, which is also of importance to assess the applicability of phosphors. With the CIF values, the color purity can be obtained by adopting the following formula:[36]

$$\text{Color purity}=\sqrt{\frac{(x-x_i)^2+(y-y_i)^2}{(x_d-x_i)^2+(y_d-y_i)^2}} \quad (8)$$

where (x, y) are the CIE coordinates of the phosphor, (x_i, y_i) are the CIE coordinates of white light (0.3101, 0.3162) standardized by the National Television Standards Committee (NTSC), and (x_d, y_d) are the coordinates under main wavelength monitoring. Furthermore, the CCT of the phosphor can be calculated as follows:[37]

$$n=\frac{(x-x_e)}{(y-y_e)} \quad (x_e=0.332,\ y_e=0.186) \quad (9)$$

$$\text{CCT}=-449n^3+3535n^2-6823n+5520 \quad (10)$$

Via the formulae presented above, values of the CIE, color purity and CCT were achieved and are summarized in Table 1. With the increase of Eu^{3+} concentration, the luminous color of the NLMO:0.01Dy^{3+},yEu^{3+} series changes from green to yellow and finally to orange-red. For the CIE parameters, the x value accelerates, but the y value declines. The CCT takes the same trend as the Eu^{3+} concentration increases. However, the color purity features differently. It first increases and then decreases, peaking at y = 0.07 with the altitude value of 65%. All the above experimental and computed results hint that multi-color tunable emission with wide application prospects in the field of color display and lighting is easily realized by adjusting the ratio of Dy^{3+} and Eu^{3+} concentration.

Fig. 10(b) shows the naked eye observation images of NLMO:0.01Dy^{3+},yEu^{3+} (y = 0, 0.01, and 0.07) phosphors under commercially available violet flashlight, respectively. As one can see from the pictures, the phosphor with single doped Dy^{3+} emits dazzling green light and, when a small amount of Eu^{3+} ions (1 at%) was introduced, the color of the phosphor turns to light orange. In particular, when Eu^{3+} ions reach 7 at%, the color of the phosphor changes to red completely. This further demonstrates the great potential of this phosphor in W-LED and color display applications.

4. Conclusions

In summary, a series of Dy^{3+} single-doped and Dy^{3+},Eu^{3+} co-doped NLMO phosphors were prepared by an EDTA–2Na

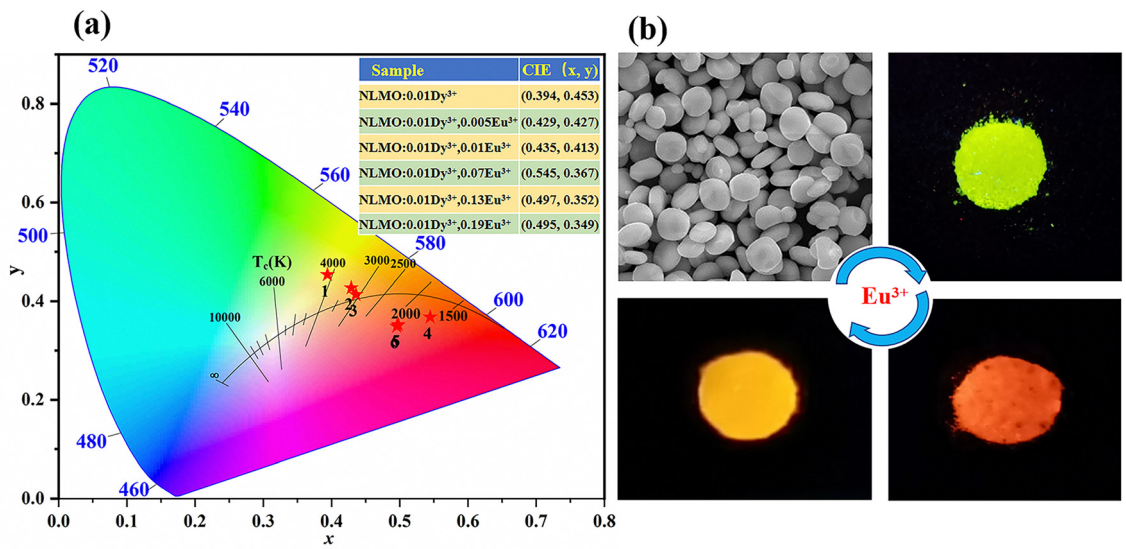

Fig. 10 (a) CIE diagram of NLMO:0.01Dy^{3+}yEu^{3+} (y = 0, 0.005, 0.01, 0.07, 0.13, and 0.19) phosphors and (b) naked-eye observation of luminescence performance of the NLMO:0.01Dy^{3+},yEu^{3+} (y = 0, 0.01, and 0.07) phosphors under the excitation of commercially available violet flashlight.

Table 1 CIE, CCT and color purity for the NLMO:0.01Dy^{3+},yEu^{3+} phosphors

Method	CIE	CCT (K)	Color purity (%)
NLMO:0.01Dy^{3+}	(0.394, 0.453)	4120	31
NLMO:0.01Dy^{3+},0.005Eu^{3+}	(0.429, 0.427)	3316	44
NLMO:0.01Dy^{3+},0.01Eu^{3+}	(0.435, 0.413)	3109	44
NLMO:0.01Dy^{3+},0.07Eu^{3+}	(0.545, 0.367)	1640	65
NLMO:0.01Dy^{3+},0.13Eu^{3+}	(0.497, 0.352)	1779	52
NLMO:0.01Dy^{3+},0.19Eu^{3+}	(0.495, 0.349)	1773	51

assisted hydrothermal method. The emission of Dy^{3+} ions at two characteristic peaks of 469 nm and 573 nm was observed in the NLMO:xDy^{3+} phosphors excited at 355 nm. Through calculation and data fitting, dipole–dipole interaction takes the main role in the concentration quenching mechanism of Dy^{3+}. In addition, the emission color of Dy^{3+} and Eu^{3+} co-doped NLMO phosphors can be adjusted from yellow to green and finally to orange-red by adjusting the ratio of Dy^{3+} to Eu^{3+} ion concentrations. As the concentration of Eu^{3+} increases, ranging from 1 at% to 19 at%, the process of energy transformation from Dy^{3+} to Eu^{3+} significantly enhances with corresponding energy transfer efficiencies of 15.64%, 25.5%, 57.79%, 88.82%, and 90.32%, respectively. The appropriate concentrations of Dy^{3+} and Eu^{3+} were determined to be 1 at% and 7 at%, respectively. The lifetimes of the NLMO:0.01Dy^{3+},yEu^{3+} (y = 0, 0.005, 0.01, 0.07, 0.13, and 0.19) phosphors gradually decreased with the increase of Eu^{3+} concentration. Luminous thermal stability of the studied phosphors was investigated with the NLMO:0.01Dy^{3+} and NLMO:0.01-Dy^{3+},0.07Eu^{3+} phosphors as examples. The luminescence intensity at 423 K for the former remained at 59% compared to that at room temperature while the value reached as high as 97% due to the cooperation effect of Eu^{3+}, indicating the crucial role of Eu^{3+} in the preservation of luminescence intensity at a higher temperature. The CCT values of the NLMO:0.01Dy^{3+},yEu^{3+} (y = 0, 0.005, 0.01, 0.07, 0.13, and 0.19) phosphors gradually decrease from 4120 K when y = 0 to 1649 K as y = 0.07. In summary, the NLMO:0.01Dy^{3+},yEu^{3+} (y = 0, 0.005, 0.01, 0.07, 0.13, and 0.19) phosphors possess excellent multi-color tunable ability with high performance in the aspect of thermal stability, enabling them to have much potential applications in color displays and various other fields.

Data availability

The data that support the findings of this study are available upon reasonable request.

Conflicts of interest

The authors declare that they have no known competing financial interests or personal relationships that could have appeared to influence the work reported in this paper.

Acknowledgements

This work was supported by the National Natural Science Foundation of China (12264004), the Natural Science Foundation of Jiangxi Province (20202ACBL214020 and 20224BAB204029), the Science and Technology Research Project of Jiangxi Provincial Education Department (GJJ211412), Scientific Research Based Project of Gannan Normal University (2020KY11) and the US National Science Foundation (DMR-1904701).

References

1 J. L. Zhang, Y. N. He, Z. X. Qiu, W. L. Zhang, W. L. Zhou, L. P. Yu and S. X. Lian, Site-sensitive energy modes in $Ca_3Al_2O_6$: Ce^{3+}/Tb^{3+}/Mn^{2+} phosphors, *Dalton Trans.*, 2014, **43**(48), 18134–18145.
2 M. Y. An, J. B. Cui, Q. He and L. Y. Wang, Down-/up-conversion luminescence nanocomposites for dual-modal cell imaging, *J. Mater. Chem. B*, 2013, **1**(9), 1333–1339.
3 Y. C. Jia, Y. J. Huang, Y. H. Zheng, N. Guo, H. Qiao, Q. Zhao, W. Z. Lv and H. P. You, Color point tuning of $Y_3Al_5O_{12}$: Ce^{3+} phosphor via Mn^{2+}-Si^{4+} incorporation for white light generation, *J. Mater. Chem.*, 2012, **22**(30), 15146–15152.
4 V. R. Bandi, B. K. Grandhe, H. J. Woo, K. W. Jang, D. S. Shin, S. S. Yi and J. H. Jeong, Luminescence and energy transfer of Eu^{3+} or/and Dy^{3+} co-doped in Sr_3AlO_4F phosphors with NUV excitation for WLEDs, *J. Alloys Compd.*, 2012, **538**, 85–90.
5 Y. Shimodaira, H. Kato, H. Kobayashi and A. Kudo, Photophysical properties and photocatalytic activities of bismuth molybdates under visible light irradiation, *J. Phys. Chem. B*, 2006, **110**(36), 17790–17797.
6 P. Du and J. S. Yu, Photoluminescence and cathodoluminescence properties of Eu^{3+} ions activated $AMoO_4$(A = Mg, Ca, Sr, Ba) phosphors, *Mater. Res. Bull.*, 2015, **70**, 553–558.
7 A. García-Cortes and C. Cascales, Crystal Growth and Optical and Spectroscopic Characterization of the Ytterbium-Doped Laser Molybdate Yb-$Li_3Gd_3Ba_2(MoO_4)_8$, *Chem. Mater.*, 2008, **20**(12), 3884–3891.
8 L. Zhao, D. Y. Wang, C. X. Chen and Y. H. Wang, Synthesis and photoluminescence properties of novel CaB_6O_{10}: RE^{3+} (RE = Ce, Tb, Dy, Eu) phosphors under ultraviolet excitation, *Mater. Res. Bull.*, 2015, **70**, 817–821.
9 Y. L. Liu, H. L. Xiong, N. N. Zhang, Z. H. Leng, R. Q. Li and S. C. Gan, Microwave synthesis and luminescent properties of YVO_4: Ln^{3+} (Ln = Eu, Dy and Sm) phosphors with different morphologies, *J. Alloys Compd.*, 2015, **635**(15), 126–134.
10 D. L. Monika, H. Nagabhushana, R. H. Krishna, B. M. Nagabhushana, S. C. Sharma and T. Thomas, Synthesis and photoluminescence properties of novel Sr_2CeO_4: Dy^{3+} nanophosphor with enhanced brightness by Li+ co-doping, *RSC Adv.*, 2014, **4**(73), 38655–38662.
11 X. Y. Sun, J. C. Zhang, X. G. Liu and L. W. Lin, Enhanced luminescence of novel $Ca_3B_2O_6$: Dy^{3+} phosphors by Li+-codoping for LED applications, *Phys. Rev. B: Condens. Matter Mater. Phys.*, 2011, **406**(21), 4089–4093.

12 Y. F. Liu, Z. P. Yang, Q. M. Yu, X. Li, Y. M. Yang and P. L. Li, Luminescence properties of $Ba_2LiB_5O_{10}$: Dy^{3+} phosphor, *Mater. Lett.*, 2011, **65**(12), 1956–1958.

13 H. Q. Zuo, Y. Liu, J. Y. Li, X. L. Shi and W. P. Gao, Synthesis and luminescence properties of Eu^{3+}-doped $KLa(MoO_4)_2$ red-emitting phosphor, *Superlattices Microstruct.*, 2015, **85**, 672–679.

14 Y. Liu, H. Q. Zuo, J. Y. Li, X. L. Shi, S. Y. Ma, M. Z. Zhao, K. Zhang and C. Y. Wang, Hydrothermal synthesis and multicolor luminescence properties of Dy^{3+}/Eu^{3+} co-doped $KLa(MoO_4)_2$ phosphors, *Ceram. Int.*, 2016, **42**(6), 7781–7786.

15 B. Devakumar, P. Halappa and C. Shivakumara, Dy^{3+}/Eu^{3+} co-doped $CsGd(MoO_4)_2$ phosphor with tunable photoluminescence properties for near-UV WLEDs applications, *Dyes Pigm.*, 2017, **137**, 244–255.

16 M. Z. Zhang, L. Lin, Z. H. Feng, Z. Z. Wang, Y. M. Yang, W. J. Ma, J. Y. Cai, P. Lu, S. Y. Jia and Z. Q. Zheng, Color-tunable hypersensitive temperature sensor based on metal organic framework doped with Eu^{3+} and Dy^{3+} via phonon-assisted energy transfer, *J. Rare Earths*, 2023, **41**(11), 1662–1669.

17 J. Y. Wan, H. Y. Wu, Y. M. Li, Y. L. Chen, C. Y. Peng, G. Chen and Y. H. Hu, Boosting up color tunability of $Sr_2Ga_2GeO_7$ by energy transfer between Dy^{3+} and Eu^{3+} ions, *Opt. Mater.*, 2023, **139**, 113772.

18 Y. B. Meng, Z. Z. Lu, S. Wang, H. Fan, L. Y. Zhou, L. Yang and C. Z. Zhong, Synthesis and luminescence properties of double perovskite Bi^{3+}/Mn^{4+}co-doped Ca_2GdTaO_6 phosphor, *J. Lumin.*, 2021, **233**, 117898.

19 Z. W. Zhang, X. H. Shen, Y. S. Peng, Y. J. Ren and Z. Y. Mao, Tunable white light emission from single-phased Li_2SrSiO_4: Dy^{3+} phosphors by co-doping with Eu^{3+}, *Luminescence*, 2015, **30**(1), 72–78.

20 Y. X. Liu, G. X. Liu, X. T. Dong, J. X. Wang and W. S. Yu, Tunable photoluminescence and magnetic properties of Dy^{3+} and Eu^{3+} doped $GdVO_4$ multifunctional phosphors, *Phys. Chem. Chem. Phys.*, 2015, **17**(40), 26638–26644.

21 R. J. Yu, D. S. Shin, K. Jang, Y. Guo, H. M. Noh, B. K. Moon, B. C. Choi, J. H. Jeong and S. S. Yi, Photoluminescence properties of novel host-sensitized Y_6WO_12: Dy3+ phosphors, *J. Am. Ceram. Soc.*, 2014, **97**(7), 2170–2176.

22 Y. Tian, B. J. Chen, B. N. Tian, R. N. Hua, J. S. Sun, L. H. Cheng, H. Y. Zhong, X. P. Li, J. S. Zhang, Y. F. Zheng, T. T. Yu, L. B. Huang and Q. Y. Meng, Concentration-dependent luminescence and energy transfer of flower-like $Y_2(MoO_4)_3$: Dy^{3+} phosphor, *J. Alloys Compd.*, 2011, **509**(20), 6096–6101.

23 H. X. Guan, G. X. Liu, J. X. Wang, X. T. Dong and W. S. Yu, Tunable luminescence and energy transfer properties of $NaGdF_4$: Dy^{3+},Eu^{3+} nanophosphors, *New J. Chem.*, 2014, **38**(10), 4901–4907.

24 J. Liang, P. Du, H. Guo, L. L. Sun, B. Li and X. Y. Huang, High-efficiency and thermal-stable $Ca_3La(GaO)_3(BO_3)_4$: Eu^{3+} red phosphors excited by near-UV light for white LEDs, *Dyes Pigm.*, 2018, **157**(1), 40–46.

25 Y. P. Niu, F. G. Wu, Q. Zhang, Y. Teng, Y. Q. Hang, Z. Yang and Z. F. Mu, Luminescence and thermometry sensing of Sr_2InTaO_6: Eu^{3+}, Mn^{4+} phosphors in a wide temperature range, *J. Lumin.*, 2024, **275**, 120748.

26 Y. Y. Liu, J. Gao, W. Shi, X. Y. Feng, Z. J. Zhou, J. X. Wang, J. L. Guo, R. Y. Kang, B. Deng and R. Y. Yu, Deep-red-emitting Mg_2InSbO_6: Mn^{4+} phosphors with a double-perovskite structure for plant-cultivation LEDs: Synthesis and photoluminescence properties, *Ceram. Int.*, 2021, **47**(13), 18814–18823.

27 Devi S. Chahar, R. Dalal, J. Dalal, M. Bala, M. Dalal, J. Boora, P. Taxak, V. B. Lather and S. P. RajeshKhatkar, Color tunable nanocrystalline $SrGd_2Al_2O_7$: Tb^{3+} phosphor for solid state lighting, *Ceram. Int.*, 2019, **45**(1), 606–613.

28 J. Wang, Y. Y. Bu, X. F. Wang and H. J. Seo, A novel optical thermometry based on the energy transfer from charge transfer band to Eu^{3+}-Dy^{3+} ions, *Sci. Rep.*, 2017, **7**, 6023.

29 H. M. Wu, H. Chen, Y. F. Liu, Y. N. Lu and D. Q. Zhang, Highly uniform $NaLa(MoO_4)_2$:Eu^{3+} microspheres: microwave-assisted hydrothermal synthesis, growth mechanism and enhanced luminescent properties, *J. Mater. Sci.: Mater. Electron.*, 2014, **25**(7), 3109–3115.

30 J. H. Ou, X. L. Yang and S. G. Xiao, Luminescence performance of Cr^{3+} doped and Cr^{3+}, Mn^{4+} co-doped La_2ZnTiO_6 phosphors, *Mater. Res. Bull.*, 2020, **124**, 110764.

31 H. Zhang, H. Yang, X. Ma, G. Li, S. Liu, H. Li, J. Yang, Y. Liang and Y. Chen, Tunable dual emission of Bi^{3+} and Mn^{4+} co-doped $LaMg_{0.598}Nb_{0.402}O_3$ double perovskite via energy transfer for plant growth lighting, *Mater. Res. Bull.*, 2020, **126**, 110814.

32 Q. M. Lin, Q. Wang, M. Liao, M. X. Xiong, X. Feng, X. Zhang, H. F. Dong, D. Y. Zhu, F. G. Wu and Z. F. Mu, Trivalent Chromium Ions Doped Fluorides with Both Broad Emission Bandwidth and Excellent Luminescence Thermal Stability, *ACS Appl. Mater. Interfaces*, 2021, **13**(15), 18274–18282.

33 Y. H. Xu, L. Zhang, L. P. Dong, S. W. Yin, X. D. Wu and H. P. You, Novel $SrGd_2Al_2O_7$: Mn^{4+},Nd^{3+} and Yb^{3+} phosphors for c-Si solar cells, *Dalton Trans.*, 2021, **50**(20), 7017–7025.

34 Z. W. Zhou, J. M. Zheng, R. Shi, N. M. Zhang, J. Y. Chen, R. Y. Zhang, H. Suo, E. M. Goldys and C. F. Guo, Ab initio site occupancy and far-red emission of Mn^{4+} in cubic-phase $La(MgTi)_{1/2}O_3$ for plant cultivation, *ACS Appl. Mater. Interfaces*, 2017, **9**(7), 6177–6185.

35 J. H. Hong, Y. Liu, Y. C. Xu, X. G. Meng, H. S. Fan, J. Li and Z. P. Lin, Luminescence properties and energy transfer study of color temperature tunable $CaSrSiO_4$: Dy^{3+}, Eu^{3+} white phosphors, *Opt. Mater.*, 2024, **149**, 115033.

36 S. Wang, Y. J. Han, L. Shi, M. X. Jia, W. Y. Zhang, Y. L. Tong, Z. F. Mu and Z. W. Zhang, A new strategy to the $NaY(MoO_4)_2$: Eu^{3+} phosphors modified by tetraethyl orthosilicate for LEDs: Photoludminescence properties and morphology, *Optik*, 2020, **217**, 164872.

37 Y. Parganiha, J. Kaur, V. Dubey, R. Shrivastava and S. J. Dhoble, Synthesis and luminescence study of $BaZrO_3$: Eu^{3+} phosphor, *Superlattices Microstruct.*, 2015, **88**, 262–270.